Water molecule by the self-consistent atomic deformation method

M. M. Ossowski, L. L. Boyer, M. J. Mehl, and M. R. Pederson
Center for Computational Materials Science, Naval Research Laboratory, Washington, DC 20375, USA
(Received 28 May 2003; revised manuscript received 15 September 2003; published 11 December 2003)

We present a density functional method which expresses the charge density of a system of atoms as a sum over localized atomiclike densities derived from potentials defined variationally from the total energy expression, which includes contributions from overlapping densities. An approach for systematically increasing the variational freedom of the atomiclike densities is introduced and tested for the water molecule. For the water molecule our method results in complete charge transfer for sufficiently small bond lengths and reverses the charge transfer at large bond lengths. In case of complete charge transfer the overlap contributions are zero, allowing a direct comparison with the traditional Kohn–Sham approach.

DOI: 10.1103/PhysRevB.68.245107 PACS number(s): 71.15.Mb, 77.22.Ej, 63.20.Dj

I. INTRODUCTION

The self-consistent atomic deformation (SCAD) method has been recently developed as an efficient application of the density functional theory (DFT) in the framework of localized charge density.[1] In our method the densities are obtained self-consistently by solving one-electron Schrödinger equations, for each atomic site, whose potentials are determined variationally from the total energy. As a consequence, we introduce an approximate kinetic energy functional T_k to account for the extra contribution from the overlapping charge densities.

For ionically bonded systems SCAD provides a picture of the electronic structure that prohibits the transfer of charge from one ion to another. Thus, the polarization and related properties are unambiguously given by the induced dipole moments of the ions.[2] This is illustrated by results of calculations on a variety of systems; alkali halides,[3] oxide-based perovskides,[4,5] MgO and AlP,[1] $Ba_2Al_2O_4$,[6] and α-Al_2O_3.[7]

For systems like the water molecule SCAD may require the full transfer of electrons off the hydrogen atoms in which case the charge overlap is zero and, in principle, the only approximation present is the LDA. Of course, this assumes that the single-center basis set is adequate. The purpose of this work is to show that, by adding a procedure to systematically improve the basis set, single-center accurate solutions for such systems are computationally feasible.

II. METHOD

In the SCAD method the total electronic charge density of the system is the sum of the overlapped site localized densities

$$n(\mathbf{r})=\sum_i n_i(\mathbf{r}-\mathbf{R}_i)=\sum_i \sum_{l,m} n_{lm}^{(i)}(|\mathbf{r}-\mathbf{R}_i|)Y_{lm}(\widehat{\mathbf{r}-\mathbf{R}_i}), \tag{1}$$

and the total energy is written as

$$E[n(\mathbf{r})]=\sum_i T_0[n_i(\mathbf{r})]+T_k[n(\mathbf{r})]-\sum_i T_k[n_i(\mathbf{r})] + F[n(\mathbf{r})]. \tag{2}$$

In the above expression $T_0[n_i(\mathbf{r})]$ is the kinetic energy of a set of noninteracting electrons centered about the atomic site at $\mathbf{R}_i$ and $F[n(\mathbf{r})]$ contains exchange-correlation[9] and electrostatic contributions to the total energy. The overlap kinetic energy $T_k[n(\mathbf{r})]$ is approximated by the simple Thomas–Fermi expression

$$T_k[n(\mathbf{r})]=\frac{3}{5}(3\pi^2)^{2/3}\int n^{3/5}(\mathbf{r})d^3r. \tag{3}$$

We thus have reduced the general problem into a much easier task of sequentially (or in parallel) solving single-particle Schrödinger's equations for each atomic site at $\mathbf{R}_i$ with the corresponding potentials derived variationally from the total energy[10]

$$v_i(\mathbf{r})=\frac{\delta E[n(\mathbf{r})]}{\delta n_i(\mathbf{r})}=v_F[n(\mathbf{r})]+v_k[n(\mathbf{r})]-v_k[n_i(\mathbf{r})] =\sum_{l,m} v^{(i;l,m)}(r)Y_{lm}(\hat{\mathbf{r}}), \tag{4}$$

where

$$v_F[n(\mathbf{r})]=\frac{\delta F[n(\mathbf{r})]}{\delta n(\mathbf{r})} \tag{5}$$

is the functional derivative of $F[n(\mathbf{r})]$ equal to the Kohn–Sham potential and

$$v_k[n(\mathbf{r})]=\frac{\delta T_k[n(\mathbf{r})]}{\delta n(\mathbf{r})}. \tag{6}$$

If we assume that all the charge density is localized on nonoverlapping sites, then

$$T_k[n(\mathbf{r})]=\sum_i T_k[n_i(\mathbf{r})], \tag{7}$$

and the expression Eq. (2) reduces to the familiar Hohenberg and Kohn form.[8]

A variety of numerical techniques are employed in calculating this potential. Here we outline the procedure for the case of a water molecule. Although we will show later that in

the case of H_2O the SCAD picture is completely ionic, which leaves the hydrogen atoms without electrons and reduces the overlap to zero [cf. Eq. (7)], we do not make such an assumption *a priori*. This completely ionic picture is valid when the hydrogen nuclei are close to the oxygen atom. However, for separation distances of more than twice the equilibrium bond length some charge must be transferred back to minimize energy in accord with Janak's theorem (see below).

Therefore, we start by defining the overlap potential as $v_{ov}=v_k+v_{xc}$ and rewriting Eq. (4) as

$$v_i(\mathbf{r})=v_{es}[n(\mathbf{r})]+v_{xc}[n_i(\mathbf{r})]+v_{ov}[n(\mathbf{r})]-v_{ov}[n_i(\mathbf{r})]. \tag{8}$$

Two features of the overlap potential complicate expressing it in spherical harmonics: (1) it has sharp features near atomic nuclei at $\mathbf{R}_j$ and (2) unlike the electrostatic contribution, it does not naturally decompose into additive terms from each site. Both complications are simplified by computationally adding and subtracting $\Sigma_j' v_{ov}[n_0^{(j)}(\mathbf{r})]$, where n_0 denotes the $l=0$ portion of the density and the prime on the summation indicates that the $j=i$ term is omitted. The subtracted part combines with the last two terms of Eq. (8) to give a contribution which is smoothly varying near $\mathbf{R}_j$, while the added part is combined with the electrostatic contribution due to $n_0^{(j)}(\mathbf{r})$ and treated using the Löwdin[13] transformation. The $l>0$ electrostatic contributions due to the nonspherical components of $n^{(j)}(\mathbf{r})$ at $\mathbf{R}_j$ are included in the smooth part, as is also the $l>0$ portion of $v_{xc}[n_i(\mathbf{r})]$, namely $v_{xc}[n_i(\mathbf{r})]-v_{xc}[n_0^{(i)}(\mathbf{r})]$.

Our potential for the ith atom can now be rewritten as

$$v_i(\mathbf{r})=v_{on}^i(\mathbf{r})+v_s^i(\mathbf{r})+v_L^i(\mathbf{r})+v_n^i(\mathbf{r}), \tag{9}$$

with subscripts denoting onsite, smooth, Löwdin and nuclear parts.

The onsite part

$$v_{on}^i(\mathbf{r})=v_{xc}[n_0^{(i)}(\mathbf{r})]+\int \frac{n_i(\mathbf{r}')}{|\mathbf{r}-\mathbf{r}'|}\,d\mathbf{r}'-\frac{Z_i}{r}, \tag{10}$$

using Hartree units ($e=m=1$), is easily computed using the $1/|\mathbf{r}-\mathbf{r}'|$ addition theorem for angular integrations and by numerically performing remaining radial integrations. The resultant spherical harmonic expansion coefficients $v_{on}^{(i;l,m)}(r)$ [cf. Eq. (4)] are kept on a fine logarithmic mesh of several hundred points.

The smooth part of the potential

$$v_s^i(\mathbf{r})=v_{xc}[n_i(\mathbf{r})]-v_{xc}[n_0^{(i)}(\mathbf{r})]+v_{ov}[n(\mathbf{r})]-v_{ov}[n_i(\mathbf{r})] -\Sigma_j' v_{ov}[n_0^{(j)}(\mathbf{r})]+\Sigma_j'(v_{es}[n_j(\mathbf{r})]-v_{es}[n_0^{(i)}(\mathbf{r})]) \tag{11}$$

is computed by interpolating the v_{es} and density contributions from the neighboring atoms to a coarse logarithmic radial mesh centered at site i. Typically, the coarse mesh comprises ~ 30 radial points and ~ 150 directions. Therefore for the water molecule with the oxygen (density) potential computed up to $l=12$ we have $\geqslant 0.8$ million interpolations per hydrogen atom. This is a substantial part of the SCAD calculation. The directions and weights of the coarse mesh are generated similarly to those of Gaussian quadrature to facilitate efficient angular integrations[14]

$$v_s^{(i;l,m)}(r)=\int v_s^{(i)}(r)Y_{l,m}^*(\hat{\mathbf{r}})\,d\Omega. \tag{12}$$

The coefficients $v_s^{(i;l,m)}(r)$ are further interpolated from the coarse to the dense mesh completing the calculation of the spherical harmonics expansion of the smooth part of the potential.

The Löwdin part of the potential

$$v_L^{(i)}(\mathbf{r})=\sum_j{}' \,(v_{ov}[n_0^{(j)}(\mathbf{r})]+v_{es}[n_0^{(j)}(\mathbf{r})]) \tag{13}$$

is computed by transforming the spherically symmetric function $v_{ov(es)}[n_0^{(j)}(r'^{(j)})]Y_{0,0}$ to a spherical harmonic expansion about the new origin at the site i separated a distance $a^{(j)}$ along the z axis[13]

$$v_{ov(es)}[n_0^{(j)}(\mathbf{r})]=\sum_l g_l^{(j)}(r)Y_{l,0}(\hat{\mathbf{r}}), \tag{14}$$

where

$$g_l^{(j)}(r)=\sqrt{2l+1}\int_0^\pi v_{ov(es)}[n_0^{(j)}(r'^{(j)})]P_l(\cos\theta)\sin(\theta)\,d\theta \tag{15}$$

and

$$r'^{(j)2}=r^{(j)2}+a^2-2a^{(j)}r\cos(\theta), \tag{16}$$

followed by an appropriate transformation by the polar angle θ. Here r' refers to coordinates with respect to the old origin. Expression Eq. (15) can be evaluated by numerical integration, provided special care is exercised close to site j where the slope of $g_l^{(j)}$ is discontinuous and where a finer integration step leads to increasingly sharp features. We overcome this difficulty by expanding Eq. (15) in terms of $\sqrt{2l+1}/(2a^{(j)}r)^{l+1}$ times appropriate combinations of integrals of type[12]

$$I_l^{(j)}(r)=\int_{|a^{(j)}-r|}^{r+a^{(j)}} f(x)x^{2l+1}\,dx. \tag{17}$$

These integrals can be conveniently interpolated from tabulated values. However, because of the presence of the factor $\sqrt{2l+1}/(2a^{(j)}r)^{l+1}$ the expansion becomes numerically unstable for small values of r. In this region we expand the $f(x)$ in Eq. (17) in a Taylor series about $a^{(j)}$ and perform the integrations analytically. Values for $f^{(n)}$ are determined numerically from $f^{(n-1)}$ using a 5-point interpolation formula.[15] We match the small r solutions and large r solutions in the region where they are both accurate. This mixing occurs at a few tenths of a Bohr and is somewhat further out for larger l values.

The potential due to neighboring nuclei,

$$v_n^{(i)}(\mathbf{r}) = \sum_j{}' \frac{Z_j}{|\mathbf{r}-\mathbf{R}_j|}, \tag{18}$$

is given by the $1/|\mathbf{r}-\mathbf{R}_j|$ addition theorem. Here the sum over j excludes the $j=i$ term, already included in the onsite part. The nuclear potential can also be included as a part of the Löwdin potential, as we have done to test the code.

Both the Löwdin and the nuclear part of the potential contain discontinuities in the radial derivatives at $\mathbf{R}_j$. Therefore we have to be extra careful when evaluating the Hamiltonian matrix elements and the total energy. Our strategy is to omit contributions to v_L and v_n due to $\mathbf{R}_j$ for a selected number of fine mesh points around the peak at $\mathbf{R}_j$ and instead compute v_L and v_n at radii given by Gaussian quadratures on both sides of the peak. Typically, only a few Gaussian points are needed on each side of $\mathbf{R}_j$. Values for v_L are then obtained by interpolation from values for the integral Eq. (17) already computed on the logarithmic mesh. To calculate the total energy (expressed in terms of integrals over nv) the corresponding values for the charge density where v_L and v_n have sharp features must also be computed.

Once the potential for each site i is computed the associated one-electron Schrödinger equations are solved. The lowest energy levels for the entire system are occupied by the available electrons in accord with Janak's theorem.[18] This supplies new densities $n_i(\mathbf{r})$ and the procedure is repeated, with optimal mixing of new and old densities, until self-consistency is reached. The one-electron Schrödinger equations are solved using a flexible set of SCAD basis functions. For each site we include the atomic orbitals of a free atom[16,17] plus sets of Slater ($r^l e^{-\beta_i r} Y_{l,m}$) or Gaussian ($r^l e^{-\alpha_i r^2} Y_{l,m}$) functions $\phi_i(r)$. We use the "even tempered" Slater (Gaussian) functions for which the temperment t defined as

$$t = 4\pi \int_0^\infty r^2 \phi_i(r)\, \phi_{i+1}(r)\, \mathrm{d}^3 r \tag{19}$$

is constant for a given l. The number of functions included can be adjusted, by parameters t and r_0—orbital cutoff radius which represents the radius of the peak of the outermost Slater or Gaussian, to meet the convergence criteria. The analytic form of the hydrogenlike wave functions suggests that for small values of l $\beta_1 = Z/(l+1)$ [$\alpha_1 = \beta_1^2/2(l+1)$ for Gaussian sets]. Since the optimized Slater-type bases for atoms generally include somewhat larger values for β we also include an additional $i=0$ ($\beta_0 > \beta_1$) function in our basis. For larger values of l the exponent β_1 is determined from the radius of the outermost peak of the highest energy occupied atomic orbital as tabulated in the atomic data tables.[16,17] In this case we add the $i=0$ (β_0) function as well.

III. THE WATER MOLECULE

The SCAD method described above and expanded to include long-range Coulomb interactions was previously applied to study the lattice dynamics and elastic properties of corundum, α-Al_2O_3.[7] However, in that work our basis functions were limited to those with radial dependence given by Slater functions as tabulated by Clementi and Roetti. Here we present a case of a water molecule to illustrate the flexibility of our newly developed basis set. We demonstrate that SCAD's results converge to those obtained with the state-of-the-art, linear combination of Gaussian orbital method (NRLMOL)[19–21] in the high $l_{\max}$ limit and consequently, for water, our method leads to results identical with the Kohn and Sham formulation of DFT.[11] In both methods we use the LDA approximation of Perdew and Wang.[22]

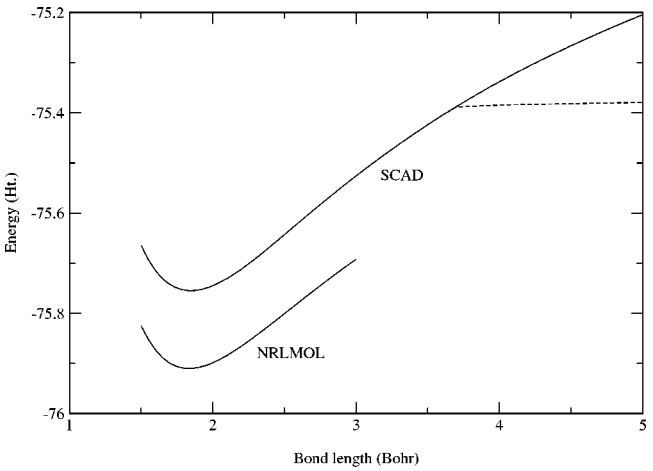

FIG. 1. Total energy as a function of bond length r, at fixed bond angle, $\theta = 105.2°$, for the water molecule obtained by SCAD and NRLMOL. The dashed SCAD curve corresponds to charge transfer back to H^+ ions in order to minimize the energy. Here and in Figs. 2–4 SCAD $l_{\max}=3$.

We compute the H_2O total energy as a function of bond length r at the SCAD approximate ($l_{\max}=10$) equilibrium bond angle θ of 105.2°. Unless otherwise indicated, in the following, all the calculations are carried out for $l_{\max}=3$ at the approximate SCAD minimum of bond length of 1.833 Bohr and bond angle of 105.2°. Figure 1 compares the total energy obtained by SCAD in the interval between 1.5 and 5 Bohrs with the results obtained from NRLMOL. The SCAD minimum occupied energy levels are -18.587, -0.906, -0.458, -0.327 and -0.262 (-18.608, -0.919, -0.481, -0.342, -0.270 for $l_{\max}=10$) compared with NRLMOL values of -18.611, -0.921, -0.485, -0.344, and -0.270. Energy values are in hartrees. The lowest energy levels calculated by SCAD were obtained by completely transferring the hydrogen electrons to the oxygen. In this case the lowest H^+ eigenvalue is -0.002 (-0.000 for $l_{\max}=10$), well above the highest occupied eigenvalue of O^{2-}. The SCAD picture of the H_2O molecular bonding is thus that of an O^{2-} ion in the potential of two protons. This picture is not easily changed, as seen from Fig. 1, where the total energy starts being lowered by transferring charge back to the oxygen atom only at very large bond lengths above 3.5 Bohr.

The effect of charge transfer is further described in Figs. 2–4. We notice that the lowest eigenvalue of H^+ (dashed curve in Fig. 2) intersects the mean energy of the occupied

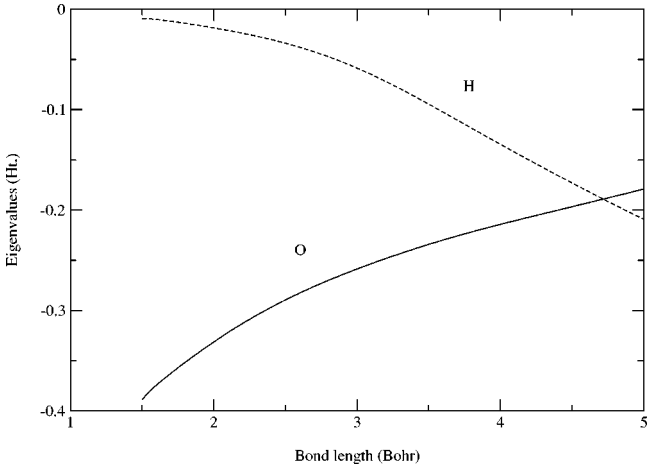

FIG. 2. SCAD averaged $2p$ occupied eigenvalues of O^{2-} and the lowest eigenvalue of H^{+} (dashed curve) as a function of bond length r, at fixed bond angle, $\theta = 105.2°$, for the water molecule. No charge is transferred back to the hydrogen ions.

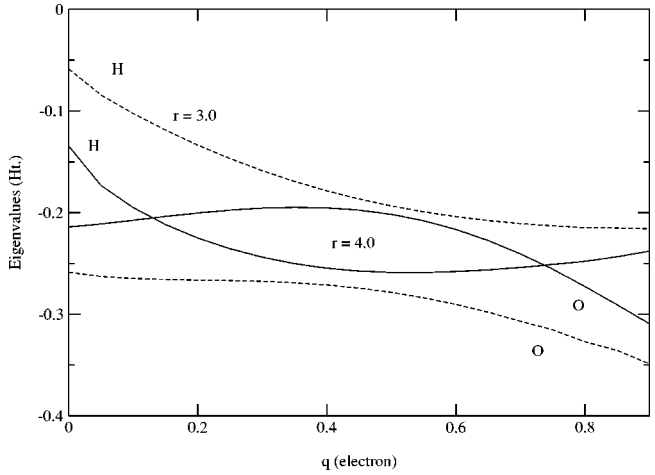

FIG. 4. SCAD mean energy of the $2p$ occupied levels of O^{-2+2q} and the lowest energy level of H^{+1-q} as a function of the fraction of an electron charge on the hydrogen ion for two bond lengths $r = 3.0$ Bohr (dashed curves) and $r = 4.0$ Bohr (solid curves) for the water molecule, $\theta = 105.2°$.

$2p$ levels of O^{2-} (we transfer electrons in equal amounts to the three distinct $2p$ levels of oxygen to assure consistency at large bond lengths) at a point that is further out from the O^{2-} than the critical value of bond length, r_t, for which a charge transfer back to H^{+} lowers the total energy in Fig. 1. This is simply because Fig. 2 does not actually incorporate a charge transfer back to the H^{+} ions; it merely shows that such transfer is required by SCAD at some (large) value of bond length. This is the right behavior, since we expect SCAD to result in dissociation of the bonds when the oxygen and the hydrogen atoms are far apart.

It is known that certain ionic systems do not properly dissociate into atoms with integer charge within some approximations to DFT. For example, the LDA used here predicts that a LiF dimer with an essentially infinite bondlength is spin unpolarized and has charges of 2.6 and 9.4 on the Li and F, respectively. This state lies approximately 0.037 Ht below the polarized state with integer charges of 3.0 and 9.0. For LiF, GGA does not improve the results and self-interaction corrections[23,24] (SIC) are required to fix this problem. However, it is the relative sizes of the SIC shifts for valence electrons on different atoms which determine whether improper dissociation of a given system is expected to occur. We have ascertained that both LDA and GGA allow for dissociation of H_2O into spin-polarized isolated atoms with the correct integer values. It is worth noting that improvement for all pairs of atoms can be expected from recent development of hyper-GGA functionals[25] and modern hybrids[26–28] applied in the framework of the optimized effective potential method.[29–31]

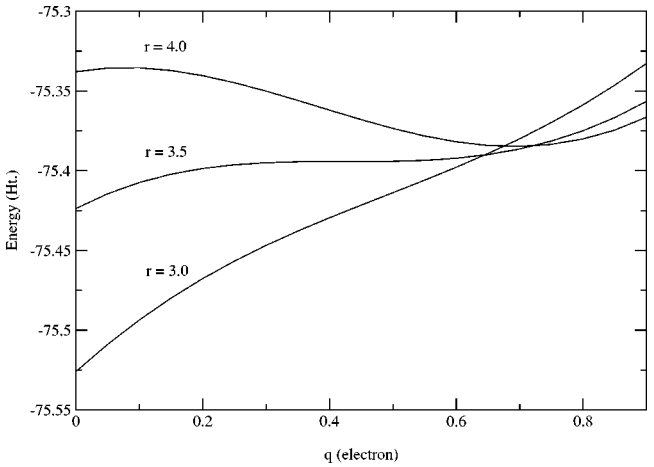

FIG. 3. SCAD total energy as a function of a fraction of an electron charge q on the hydrogen ion for the water molecule, $\theta = 105.2°$. Curves for three distinct bond lengths $r = 3.0$ Bohr, $r = 3.5$ Bohr, and $r = 4.0$ Bohr are shown.

To better understand the critical value r_t we refer to Fig. 3. In this figure we show the SCAD total energy as a function of the charge transfer for three values of bond length, $r = 3.0$ Bohr—markedly lower, $r = 3.5$ Bohr—slightly lower and $r = 4.0$ Bohr—markedly higher than r_t. For $r = 3.0$ Bohr the charge transfer back to the H^{+} ions clearly does not result in lowering of the total energy. On the contrary, an attempt to transfer any amount of charge raises the energy sharply. This situation starts to change when we approach r_t. There now exists a ''flat'' region where the increase of the amount of the charge transferred back to H^{+} does not change the total energy substantially. For $r = 3.5$ Bohr, however, the total energy for the $H_2^{+}O^{2-}$ system is still lower that the total energy of the $H_2^{+1-q}O^{-2+2q}$ system, regardless of q. If we now increased the bond length slightly we would see the local minimum in the total energy beginning to form in the ''flat'' region for a certain value of q (not shown in Fig. 3). This minimum becomes global for $r = r_t$ and for $r > r_t$ the situation is such as represented by the curve corresponding to $r = 4.0$ Bohr. The system lowers its total energy if we allow for the transfer of charge back to the

H^+ ions (in this case in the amount $q \sim 0.7$ electron/H atom).

The origin of the local maximum for the $r=4.0$ Bohr curve for oxygen at $q \sim 0.1$ electron/H atom in Fig. 3 can be understood from Fig. 4, where we once again refer to Janak's theorem.[18] As we start transferring charge back to the H^+ ions the highest occupied $2p$ states of O^{-2+2q} lie lower than the lowest allowed state of H^{+1-q}, therefore such transfer results in the increase of the total energy for both $r=3.0$ Bohr and $r=4.0$ Bohr. This situation changes for $r=4.0$ Bohr and $q > \sim 0.1$ electron/H atom when the highest occupied $2p$ states of O^{-2+2q} lie higher than the lowest allowed state of H^{+1-q}. The transfer of this amount of charge lowers the total energy in accord with Janak's theorem because doing so populates the lower eigenstates for the entire system (see Fig. 4). At $q \sim 0.7$ electron/H atom the total energy is at its global minimum, O^{-2+2q} $2p$ and H^{+1-q} $1s$ states cross again, and further transfer of charge results once again in the increase of the total energy.

For short bonds, our SCAD model requires complete charge transfer, resulting in single center expansions for the water molecule wave functions. Of course, this does not imply there is anything wrong with multicenter expansions—in fact, we compare our results with a multicenter method (NRLMOL) as a test. However, it clearly shows that concepts, such as Mulliken charges, do indeed depend on the choice of basis. Strictly speaking, the SCAD monopoles also depend on the choice of basis. For example, perversely, one could choose a nearly complete basis for the hydrogen sites and a very depleted basis for the oxygen site. If the disparity were sufficiently extreme, then the charge density near the oxygen nucleus would be constructed from hydrogen site basis functions. Clearly, this would not be a practical way to proceed. On the other hand, when similarly complete bases are chosen for all sites, SCAD monopoles have fixed integer values for nonconducting molecules and solids, which, in turn, allows relatively simple calculations for polarization.[2]

We now turn our attention to the modified basis functions. As mentioned in Sec. II we add flexibility in the basis for each l by supplementing the atomic orbitals by sets of Slater-type or Gaussian-type wave functions multiplied by appropriate spherical harmonics. This increases the number of convergence parameters. Instead of a single $l_{\max}$ we now, in addition, have for each l parameter t, which we call temperment [cf. Eq. (19)], and parameter r_0, the orbital cutoff radius. Figure 5 shows the total energy as a function of t for two sets of data. The solid line represents the energies obtained by changing t for all values of l and the broken line represents the energies obtained by changing t for all but $l=0$ and $l=1$, which we set to 0.9. We notice that the latter case better addresses the issue of small errors in the core states projecting to the larger energy difference. In both cases we see, as expected, the reduction in total energy with increased t. The value for r_0 used by us in this report is 6.0 Bohr for all l. Values higher than 6.0 Bohr do not result in significantly better wave functions, as evident from Fig. 6.

The convergence with respect to $l_{\max}$ is described in Figs. 7 and 8 which illustrate how total energy and polarization change as a function of $l_{\max}$. Clearly, these figures show that

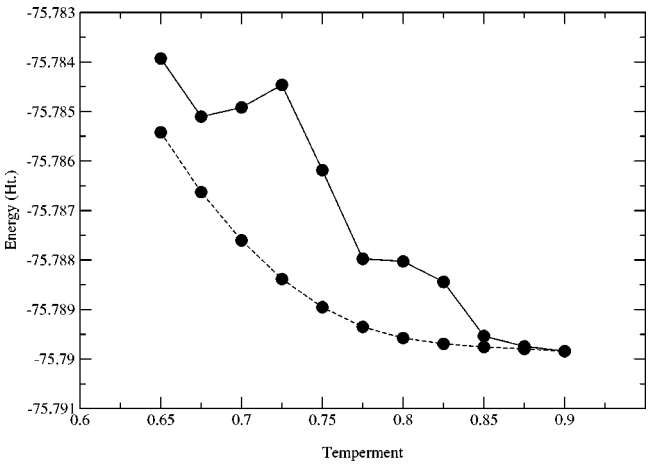

FIG. 5. Total energy as a function of temperment of the Gaussian basis functions for the water molecule, $r=1.833$ Bohr and $\theta=105.2°$. The dashed curve is for the case when t for $l=0$ and $l=1$ is set to 0.9. $r_0=6$ Bohr for all values of l.

the SCAD results converge in the limit of large $l_{\max}$, approaching those obtained with NRLMOL. This expresses the principle of the SCAD method—we can make it as exact a DFT method as allowed by the LDA and overlap kinetic energy functionals by giving the system's charge density enough variational freedom to sufficiently relax by increasing the value of $l_{\max}$ (and t and r_0).

SCAD is now fully interfaced with ISOTROPY, a software developed by Stokes, Hatch, and Wells[32,37] for applying group-theoretical methods to phase transitions in crystalline solids. In SCAD we apply ISOTROPY to construct distortion modes used in the technique for finding normal modes of oscillations in a crystal, so-called frozen phonon calculations. Our implementation of the technique uses the distortion modes which transform like basis functions of the irreducible representations (IR) of the crystal space group. This choice of the modes (which are not in general normal modes) has the effect of block-diagonalizing the dynamical matrix with each block representing a particular IR (in case of more

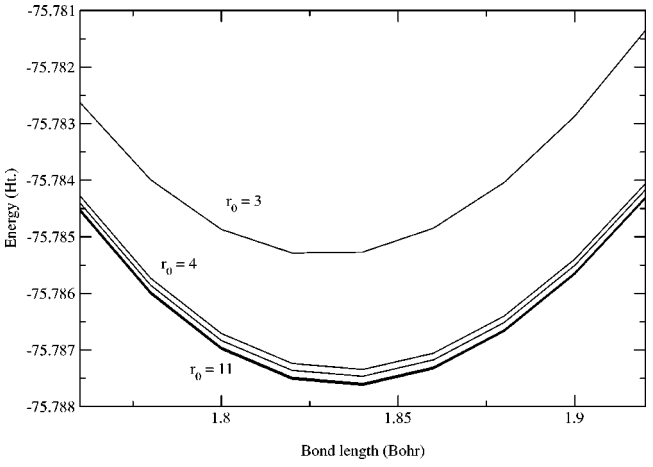

FIG. 6. Total energy as a function of bond length r, at fixed bond angle, $\theta=105.2°$, for a set of orbital cutoff radii, r_0 $(=3,4,\ldots,11)$ Bohr, for the water molecule.

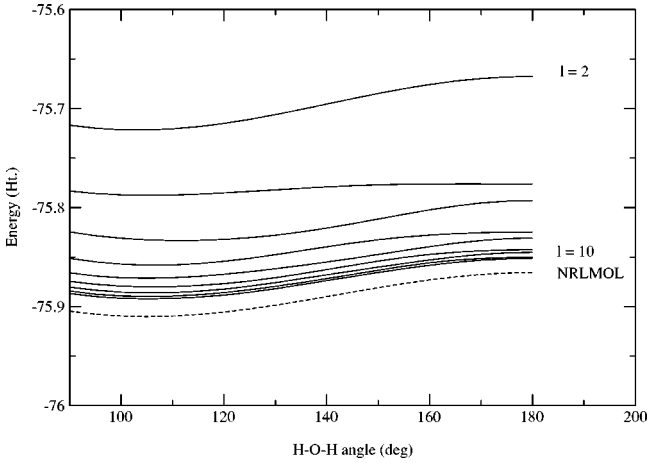

FIG. 7. Total energy as a function of bond angle θ, for a fixed bond length $r=1.883$ Bohr, for a set of $l_{\max}$ values for the water molecule. The dashed curve represents NRLMOL results.

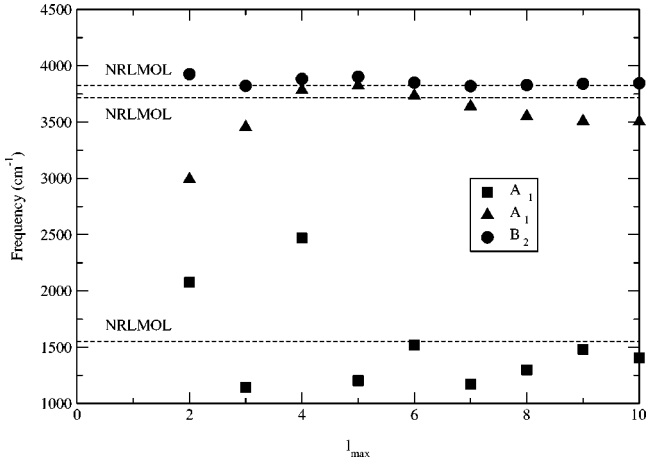

FIG. 9. SCAD vibrational frequencies for the water molecule as a function of $l_{\max}$, $r=1.833$ Bohr and $\theta=105.2°$. The dashed lines represent NRLMOL results.

than one-dimensional representation we have two or more identical blocks) and having dimension equal to the number of different distortion modes projected out by a given basis function of this IR. The elements of the dynamical matrix are calculated by SCAD as the curvatures at zero amplitude of energy parabolas for small displacements consistent with each frozen mode. In fact, to improve the accuracy we repeat these calculations with the projected modes with amplitudes consistent with eigenvectors obtained in the first pass.

In this work we want to calculate the vibrational frequencies of the isolated water molecule. We use SCAD and ISOTROPY in the same manner as described above by arranging water molecules in the crystal lattice which has the C_{2v} point group symmetry (same as the water molecule) and looking only at the Γ point. We chose the space group C_{2v}^1 ($Pmm2$, No. 25). In this group the representation Γ_1 (notation of Miller and Love[33]) corresponds to the A_1 vibrations and the representation Γ_3 corresponds to the B_2 vibration of an isolated water molecule. Therefore we calculate elements of the two blocks of the dynamical matrix consistent with these two IR's only and diagonalize them separately to obtain the normal frequencies.

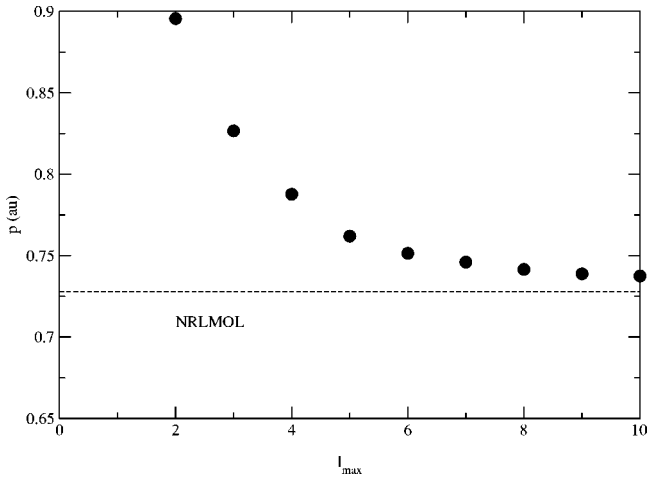

FIG. 8. Polarization as a function of $l_{\max}$ for the water molecule, $r=1.833$ and $\theta=105.2°$. The dashed line represents NRLMOL result.

The results of our calculations for values of l between 2 and 10 are shown in Fig. 9 and compared with results obtained with NRLMOL. Frequencies within NRLMOL are calculated by the so-called method of mutually orthogonal displacements. Pulay corrected Hellmann-Feynman forces are calculated for small Cartesian displacements about the equilibrium separation. The derivative of the $3N$-dimensional HF force with respect to a given displacement gives one row of the matrix of second derivatives. For each required derivative positive and negative displacements are used which ensures numerical derivatives that are accurate to fourth-order in the displacement. This allows the entire matrix of second derivatives to be determined in at most $6N$ SCF calculations. However, symmetry is used to identify the minimal number of inequivalent displacements required to determine the entire matrix of second derivatives. An early application of this method was discussed in Ref. 34. More details may be found in Ref. 35. A few fine details of the method are discussed in Ref. 36.

As it was the case for the total energy (Fig. 7) and polarization (Fig. 8) the SCAD results converge for large $l_{\max}$, approaching those obtained with NRLMOL. For $l_{\max}=10$ the errors in the frequencies are 4%, 4%, and 0% for A_1, A_1, and B_2, respectively.

IV. CONCLUSION

In this paper we report the results of precise SCAD calculations for the water molecule and compare them with those obtained from the state-of-the-art linear combination of Gaussian orbital method (NRLMOL). We demonstrate that our method results, for the water molecule, in complete charge transfer for sufficiently small bond lengths and reverses the charge transfer at large bond lengths. In the case

of complete charge transfer no charge overlap is present and SCAD and Kohn–Sham methods are equivalent in the large $l_{\max}$ limit. Our results suggest that SCAD can be applied with enough numerical precision that errors result only from the quality of the density functionals employed.

ACKNOWLEDGMENTS

The authors are grateful to Dr. T. Baruah and Dr. K. Park for helpful discussions. This work was supported by the National Research Council and the Office of Naval Research.

[1] L.L. Boyer, H.T. Stokes, and M.J. Mehl, Phys. Rev. Lett. **84**, 709 (2000).
[2] L.L. Boyer, M.J. Mehl, and H.T. Stokes, Phys. Rev. B **66**, 092106 (2002).
[3] W.N. Mei, L.L. Boyer, M.J. Mehl, M.M. Ossowski, and H.T. Stokes, Phys. Rev. B **61**, 11425 (2000).
[4] L.L. Boyer, H.T. Stokes, and M.J. Mehl, Ferroelectrics **194**, 173 (1997).
[5] L.L. Boyer, H.T. Stokes, and M.J. Mehl, in *First Principles Calculations for Ferroelectrics*, edited by R.E. Cohen, AIP Conf. Proc. No. 436 (AIP, New York, 1998), p. 227.
[6] H.T. Stokes, C. Sadate, D.M. Hatch, L.L. Boyer, and M.J. Mehl, Phys. Rev. B **65**, 064105 (2002).
[7] M.M. Ossowski, L.L. Boyer, and M.J. Mehl, Phys. Rev. B **66**, 224302 (2002).
[8] P. Hohenberg and W. Kohn, Phys. Rev. **136**, B864 (1964).
[9] L. Hedin and B.I. Lundqvist, J. Phys. C **4**, 2064 (1971).
[10] M.J. Mehl, H.T. Stokes, and L.L. Boyer, J. Phys. Chem. Solids **57**, 1405 (1996).
[11] W. Kohn and L.J. Sham, Phys. Rev. **140**, A1133 (1965).
[12] L.L. Boyer, H.T. Stokes, M.J. Mehl, and M.M. Ossowski (unpublished).
[13] G.C. Fletcher, *The Electron Band Theory of Solids* (North-Holland/American Elsevier, New York, 1971).
[14] D.C. Patton, D.V. Porezag, and M.R. Pederson, Phys. Rev. B **55**, 7454 (1997).
[15] *Handbook of Mathematical Functions*, edited by M. Abramowitz and I. Stegun (Dover, New York, 1970). (Eq. 25.3.6; Eqs. 4.2.55, 4.2.56, and 5.1.56 are used to evaluate certain radial integrations associated with v_n.)
[16] E. Clementi and C. Roetti, At. Data Nucl. Data Tables **14**, 177 (1974).
[17] A.D. McLean and R.S. McLean, At. Data Nucl. Data Tables **26**, 197 (1981).
[18] J.F. Janak, Phys. Rev. B **18**, 7165 (1978).
[19] M.R. Pederson and K.A. Jackson, Phys. Rev. B **41**, 7453 (1990).
[20] K.A. Jackson and M.R. Pederson, Phys. Rev. B **42**, 3276 (1990).
[21] D.V. Porezag and M.R. Pederson, Phys. Rev. A **60**, 2840 (1999).
[22] J.P. Perdew and Y. Wang, Phys. Rev. B **45**, 13244 (1992).
[23] J.P. Perdew and A. Zunger, Phys. Rev. Lett. **23**, 5048 (1981).
[24] M.R. Pederson and C.C. Lin, J. Chem. Phys. **80**, 1972 (1984).
[25] J.P. Perdew and K. Schmidt, in *Density Functional Theory and Its Applications to Materials*, edited by V. Van Doren *et al.* (American Institute of Physics, New York, 2001).
[26] A.D. Becke, J. Chem. Phys. **107**, 8554 (1997).
[27] J. Jaramillo, G.E. Scuseria, and M. Ernzerhof, J. Chem. Phys. **118**, 1068 (2003).
[28] J. Heyd, G.E. Scuseria, and M. Ernzerhof, J. Chem. Phys. **118**, 8207 (2003).
[29] W. Yang and Q. Wu, Phys. Rev. Lett. **89**, 143002 (2002), and references therein.
[30] S. Kummel and J. Perdew, Phys. Rev. Lett. **90**, 043004 (2003).
[31] S. Kummel and J. Perdew, Mol. Phys. **101**, 1363 (2003).
[32] H.T. Stokes, D.M. Hatch, and J.D. Wells, Phys. Rev. B **43**, 11010 (1991).
[33] S. C. Miller and W. F. Love, *Tables of Irreducible Representations of Space Groups and Co-Representations of Magnetic Space Groups* (Pruett, Boulder, 1967).
[34] A.A. Quong, M.R. Pederson, and J.L. Feldman, Solid State Commun. **87**, 535 (1993).
[35] D.V. Porezag and M.R. Pederson, Phys. Rev. B **54**, 7830 (1996).
[36] M.R. Pederson, A.A. Quong, J.Q. Broughton, and J.L. Feldman, Comput. Mater. Sci. **2**, 536 (1994).
[37] The code is available at http://128.187.202.55/~stokesh/isotropy.html